Extreme value indicators in highly resolved climate change simulations for the Jordan River area

R. Samuels,[1] G. Smiatek,[2] S. Krichak,[1] H. Kunstmann,[2] and P. Alpert[1]

Received 31 May 2011; revised 16 September 2011; accepted 14 October 2011; published 30 December 2011.

[1] Understanding changing trends and frequency of extreme rainfall and temperature events is extremely important for optimal planning in many sectors, including agriculture, water resource management, health, and even economics. For people living in the Jordan River region of the Middle East such changes can have immediate devastating impacts as water resources are already scarce and overexploited and summer temperatures in the desert regions can reach 45°C or higher. Understanding shifts in frequency and intensity of extreme events can provide crucial information for planning and adaptation. In this paper we present results from regional climate model simulations with RegCM3 and MM5 centered on the eastern Mediterranean region. Our analysis focuses on changes in extreme temperature and rainfall events. We show that maximum daily summer temperature is expected to increase by between 2.5°C and 3°C, with an increase in warm spell length. Precipitation extremes are expected to increase with longer dry spells, shorter wet spells, and increases in heavy rainfall. Model agreement for the control period 1961–1990 is higher in the southern region than in the north, perhaps because of the complex topography, suggesting that even small differences in spatial scale play an important role. In addition, we notice that the chosen global model plays an important role in determining future temperature trends, while the choice of regional climate model is critical for understanding how precipitation is expected to evolve.

Citation: Samuels, R., G. Smiatek, S. Krichak, H. Kunstmann, and P. Alpert (2011), Extreme value indicators in highly resolved climate change simulations for the Jordan River area, *J. Geophys. Res.*, *116*, D24123, doi:10.1029/2011JD016322.

1. Introduction

[2] Some of the most worrisome future impacts of expected climate change are shifts in frequency and intensity of extreme climatic events, specifically droughts and floods. Clear changes have been shown in increasing mean annual temperature and increasing or decreasing mean annual rainfall (depending on the region) [*Intergovernmental Panel on Climate Change* (*IPCC*), 2007b], as well as in extreme events in the Middle East region [*Zhang et al.*, 2005] and Mediterranean area [*Alpert et al.*, 2002]. Since these extreme events can have significant and devastating impacts at the local level, high-resolution climate projections have great value. Specifically, for agriculture and water resource planning, extreme rainfall events such as extended cold wet spells or long dry spells within a growing season can destroy crops and changes in rainfall distribution because of intense storms or increased drought period can have important consequences for optimal water resource planning and allocation. Changes in extreme temperature, such as increased heat waves, have immediate direct impacts on both society (e.g., health) and the economy (e.g., energy use). Concentrated efforts are being made at different scales to try and understand the impact of evolving climate on such extreme events. At the global level, there have been immense efforts worldwide to perform a well-coordinated set of 20th and 21st century climate change experiments for the Fourth Assessment Report (AR4) of the IPCC [*IPCC*, 2007b]. At the regional level, the World Climate Research Programme has initiated CORDEX: A Coordinated Regional Climate Downscaling Experiment as part of its strategic framework for 2005–2015 [*World Climate Research Programme*, 2009]. Both global and regional results are often downscaled to provide information at the local level [*Díez et al.*, 2005; *Kunstmann et al.*, 2007; *Robertson et al.*, 2007; *Giorgi and Lionello*, 2008; *Hertig and Jacobeit*, 2008; *Samuels et al.*, 2010]. Recently, along the lines of these efforts to understand climate change at the regional and local level, multiple regional climate models at the 18–25 km spatial scale have been realized within the GLOWA Jordan River (GLOWA JR) project (http://www.glowa-jordan-river.de). This is a multinational, interdisciplinary project focusing on sustainable water management in the region. As water resources are directly linked to rainfall, climate simulations are an important driving force for this project. The initial results of these models have recently been presented by *Krichak et al.* [2010], *Smiatek et al.* [2011], and *Krichak et al.* [2011].

[1]Department of Geophysics and Planetary Sciences, Tel Aviv University, Tel Aviv, Israel.
[2]Institute for Meteorology and Climate Research, Karlsruhe Institute of Technology, Garmisch-Partenkirchen, Germany.

0148-0227/11/2011JD016322

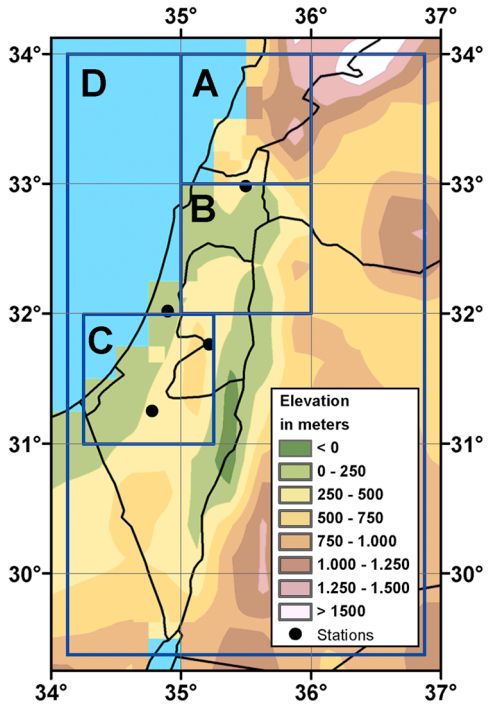

Figure 1. Study areas and locations of observed data.

[3] Given the importance of extreme climate events in general, and for the GLOWA JR project in particular, here we focus on identifying changes in specific extreme characteristics of temperature and rainfall. The indicators were chosen on the basis of core indices previously identified for extreme events [*Karl et al.*, 1999; *Peterson et al.*, 2001; *Alexander et al.*, 2006] as well as discussions with GLOWA JR colleagues and stakeholders who will use the results in hydrological, agriculture, and economic impact studies. Section 2 describes the models and data sets used as well as the study area. Section 3 describes the results of the models and presents data on extreme event frequency calculated from specific locations chosen to provide a comparison reference for the climate model results. The projected changes in the chosen indices based on the multimodel ensemble are presented here. Section 4 summarizes the central points of the study as well as provides a discussion on how this information can best be used and incorporated into environmental, societal and economic planning.

2. Material and Methods

[4] Over the past few years, the use of ensembles, or a combination of multiple climate model results, has been suggested as a way to get improved probabilistic simulations of future climate change [*Collins*, 2007]. These probabilistic scenarios can help better assess risks and are useful for planning and devising mitigation strategies [*Lopez et al.*, 2009; *Stott and Forest*, 2007]. Here we present the results of three regional climate simulations for the purpose of getting a sense of the range and variability of expected climate change. A range of model specific results as well as ensemble averages are depicted. The specific study area, observed data, climate models and chosen indicators are described below.

2.1. Study Area

[5] The study region is characterized by steep temperature and precipitation gradients because of both its complex terrain (ranging from over 2800 to −400 m) and its location at the intersection of Europe, Asia, and Africa, where it is impacted by many climatic systems. The wet season extends from October to April, followed by hot dry summer months. There is high interannual rainfall variability ranging from 60% to 125% of long-term annual average [*Alpert et al.*, 2008], limited water resources [*Gvirtsman*, 2002; *Tal*, 2006], and summer heat waves [*Saaroni et al.*, 2003]. Understanding the impacts of climate change on precipitation and temperature in the region is important for optimized planning of limited water resources, agricultural planning, and preparation for heat-induced health impacts, among other things. While most of the IPCC models simulate a decrease on rainfall in the Mediterranean, the variability between the model projections is very high [*IPCC*, 2007b; *Mariotti et al.*, 2008] hence the need for higher-resolution models.

[6] The nested regional models, which are driven by initial and boundary conditions of a single general circulation model (GCM), cannot obviously reduce the uncertainty between the different GCMs. However, the GCMs provide simulations at very rough spatial scales of 100–300 km. Many of the processes responsible for rainfall occur at much more detailed resolution, especially in the study region where orographic rainfall is so important. The nested models have the capability of capturing processes that the GCMs miss (because of their spatial resolution) and hence have the ability to represent rainfall much more accurately than their GCM counterparts.

[7] In this research, we have chosen two study regions on the basis of larger and smaller regions of impact (Figure 1). The larger region (D) encompasses the whole of the Jordan River Basin and is the main study area for the GLOWA JR project. Two smaller areas (A and B), one located in the north of Israel and one in the central area of Israel have been identified as "hot spot" areas for change in extreme precipitation conditions as they are where most of the precipitation and hence water resources are located. An additional smaller area (C) has been chosen as this includes much of central Israel where the population is most dense and increased

Table 1. Performed Simulations[a]

Institution	Abbreviation	GCM (Realization)	RCM	SVAT	DX (km)
TAU	RegCM	ECHAM5(3)	RegCM3	BATS	25
IMK-IFU	35EC5	ECHAM5(1)	MM5 V3.5	OSU LSM	18.6
IMK-IFU	37EC5	ECHAM5(1)	MM5 V3.7	Noah LSM	18.6
IMK-IFU	35had	HADCM3(1)	MM5 V3.5	OSU LSM	18.6
IMK-IFU	37had	HADCM3(1)	MM5 V3.7	Noah LSM	18.6

[a]GCM, general circulation model; DX, grid cell size; RCM, regional climate model; SVAT, surface-vegetation-atmosphere transfer model; DX, XXXX; TAU, Tel Aviv University; IMK-IFU, Institute for Meteorology and Climate Research, Karlsruhe Institute of Technology; BATS, Biosphere-Atmosphere Transfer Scheme; OSU, Oregon State University; LSM, land surface model.

Table 2. Temperature and Precipitation Statistics Used in This Study[a]

Abbreviation	Definition	Formula	Interpretation
TG	Daily mean temperature	Mean value	
TX	Daily maximum temperature	Monthly mean value of daily maximum temperature	Mean value
TXx	Monthly maximum value of daily maximum temperature	TXx = max(TX_{ik}, day i) and month k	Maximum value
TNx	Monthly minimum value of daily minimum temperature	TNx = min(TN_{ik}, day i) and month k	Minimum value
WSDI	Warm spell duration index	No. days in intervals of at least 6 days with TX > 90th percentile calculated for each calendar day (1961–1990) using running 5 day window	Count of days in runs of 6 or more days
RR	Mean precipitation		
R10	Heavy precipitation index	Number of days RR > 10 mm	Day count
R20	Very heavy precipitation index	Number of days RR > 20 mm	Day count
R75pTOT	Precipitation fraction due to R75p	Quotient of amount on days RR > 75th percentile calculated for wet days (1961–1990) and total amount	Fraction of total amount
R90pTOT	Precipitation fraction due to R90p	Quotient of amount on days RR > 90th percentile calculated for wet days (1961–1990) and total amount	Fraction of total amount
CDD	Consecutive dry days	Greatest number of consecutive days RR < 1 mm	Maximum span of days
CWD	Consecutive wet days	Greatest number of consecutive days RR ≥ 1 mm	Maximum span of days

[a]After *WMO* [2009] and http://eca.knmi.nl/documents/ETCCDMIndicesComparison.pdf.

temperature will have the most severe impact on health and quality of life.

2.2. Climate Models and Observations

[8] Recently, simulations from regional climate models focusing on the Middle East in general and the region of Israel in particular have been generated as part of GLOWA JR. The climate simulations currently include four generated in transient runs over the period 1960–2099 using two versions of the MM5 regional model (MM5 3.5 and MM5 3.7) [*Chen and Dudhia*, 2001]; one set driven by the ECHAM5 General Circulation Model (GCM) [*Roeckner et al.*, 2006] and the second driven by the UKMO (UK Meteorological Office) HadCM3 GCM [*Gordon et al.*, 2000]. The main difference between the two versions of the MM5 model used is the land surface scheme employed. Given the similarities of the two sets we averaged the results of the two sets of simulations driven by the same GCM model and present the average. Another regional climate model (RCM) simulation is performed using the International Centre for Theoretical Physics (ICTP) RegCM3 model in transient runs from 1960 to 2060 driven from the lateral boundaries by the data from ECHAM5 global climate change simulation experiment from 1850 to 2100 [*Pal et al.*, 2007; *Krichak et al.*, 2010, 2011]. Table 1 provides a list of the different models, spatial scales, and the main references for their configurations. In section 3 only three simulations are presented: (1) ECHAM5-RegCM, (2) ECHAM5-MM5, which include both MM5 simulations, and (3) HADLEY-MM5, which again includes two actual model simulations. All models results are based on the future IPCC A1B scenario which assumes technological emphasis and a balance across all energy sources.

[9] In order to better understand the skill of the model simulations for the past 1960–1990 period, we have performed comparisons with three observed data sets: (1) point data from past observations at four meteorological stations (2) gridded precipitation data provided within GLOWA JR [*Menzel et al.*, 2009] and (3) an additional gridded precipitation set from the third version of the European daily high-resolution (E-OBS Version 3.0) data for surface temperature [*Haylock et al.*, 2008; *van den Besselaar et al.*, 2011]. Both gridded data sets provide data at daily temporal resolution. GLOWA JR data were aggregated to 0.25 resolution so that they would be compatible with the E-OBS data set.

2.3. Chosen Indicators

[10] Climate change, in general, and the occurrence of extreme events in particular, is likely to impact environmental, health and other societal aspects. In this paper we focus on the changes in extreme temperature and precipitation events that have been identified as important for agriculture and water resource planning (precipitation) as well as having social and economic impacts (temperature). Specifically, as the research in this manuscript was performed as part of the GLOWA Jordan River project, these specific indicators were chosen after discussions with stakeholders, agriculturists, scientists and other professionals who are part of the project. The list of chosen indicators is presented in

Table 3. Extreme Indices Calculated at Four Meteorological Stations (1961–1990)[a]

		Station			
Index	Units	Har Kenaan	Tel Aviv	Jerusalem	Beer Sheva
TG	°C	23.4	25.2	23.4	25.8
TX	°C	29.1	28.7	28.3	32.5
TXx	°C	38.7	34.4	38.8	41.5
RR	mm	683	511	547	206
R10	mm/d	20.6	16.7	16.9	6.2
R20	mm/d	10.0	7.8	8.3	2.3
R75pTOT	%	64	63	66	64
R90pTOT	%	38	37	38	37
CDD (med)	days	26	29	29.5	36
CWD (med)	days	7	5.5	5	4

[a]The station locations area are shown in Figure 1.

Table 4. Observed Versus Simulated Model Ensemble Precipitation Statistics Averaged Over the Investigation Areas A, B, and C for the Winter Season (01.10–30.04) 1961–1990[a]

		A		B		C	
Index	Units	OBS	RCM	OBS	RCM	OBS	RCM
RR	mm	1053	1226	766	725	421	380.7
R10	mm/d	19.4	22.5	14.7	12.6	6.8	8.3
R20	mm/d	8.2	11.7	5.0	5.3	2.3	3.5
R75pTOT	%	52.8	52.4	51.6	48.9	41.4	39.8
R90pTOT	%	27.1	22.5	24.9	20.2	22.3	21.1
CDD	days	27.3	24.6	29.	30	39.3	46.1
CWD	days	7.6	7.1	7.2	5.4	5.1	4.4

[a]The observations (OBS) are from the gridded GLOWA data.

Table 2. It follows the recommendations of the *World Meteorological Organization* (*WMO*) [2009].

3. Results

[11] Initial simulation results of 1960–2060 based on the regional models used in this study have been recently published *Krichak et al.* [2010, 2011] and *Smiatek et al.* [2011]. The main findings from two simulation using RegCM (at spatial resolutions of 50 and 25 km [*Krichak et al.*, 2010, 2011]) include a notable and statistically significant precipitation drop over the near coastal EM zone during December–February and September–November and statistically significant positive air temperature trends over the entire EM region during the four seasons as well as an increase in the relative contribution of convective processes in the southern Mediterranean coastal zone region up until the year 2060. Model simulation results discussed by *Smiatek et al.* [2011] based on MM5 results indicate that compared to the control period 1960–1990, the future period 2031–2050 is expected to have an annual mean temperature 2.1°C higher than the control period and annual mean precipitation of 11.5% lower as compared to that period. Evaluation of model results for 1961–1990 show that seasonal and annual trends determined according to the results of the experiments are comparable to CRU [*Mitchell et al.*, 2004; *Mitchell and Jones*, 2005] gridded observational reference data [*Krichak et al.*, 2011] and GLOWA/E-OBS data [*Smiatek et al.*, 2011] for the same years.

[12] In this study we focus on extreme events. These events occur at the daily level and so our analysis will focus on the change in number of days per year over specific time periods, or changes in frequency or intensity percentages between two time periods. For comparison with observed data, we present in Table 3 the statistics of the chosen indicators at four rainfall stations located through out Israel (Figure 1) as well as observed versus ensemble mean statistics over the different study areas (Table 4). Extreme values for the stations (RR10, RR20, R75pTOT, and R90pTOT) are slightly higher than for the averaged areas, however, this is expected as averages naturally smooth out the peak values. In general, there is strong agreement between the gridded observed data sets and the ensemble means.

3.1. Evaluation

[13] Given the vast amounts of results generated, we have chosen to present them either as maps for the larger area D or mixed ensemble probability distributions (PDF) averaged over the smaller areas A and B for precipitation and C for temperature. The PDFs were smoothed applying the Gaussian kernel method.

3.2. Absolute and Percentile-Based Temperature Indices

[14] There are many different ways to depict and understand changes in temperature. One of the most important and interesting aspects of changing temperature is how this change differs at different spatial locations. Figure 2 shows the simulated change in maximum daily summer temperature for the larger study area and across the different models. The difference in the models can give a sense of the range of the expected changes. The Hadley/MM5 combination simulates the largest increase with 2.5°C–3°C over the whole region. The ECHAM5/MM5 shows the most modest increase

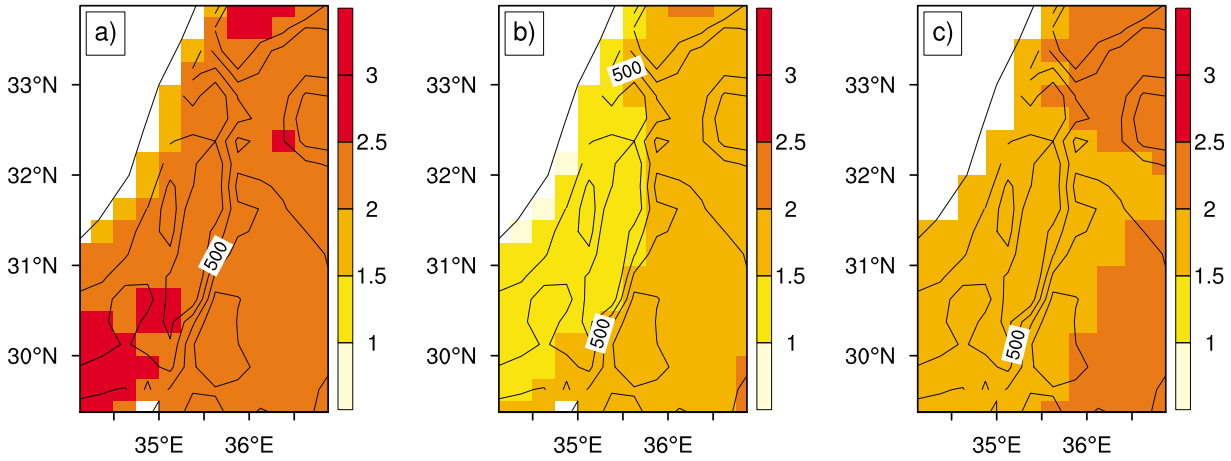

Figure 2. Simulated change in maximum daily temperature TX in °C. Summer season (June–July–August (JJA)) 2021–2050 as compared with 1961–1990. (a) MM5/HadCM3, (b) MM5/ECHAM5(1), and (c) RegCM3/ECHAM5(3). Elevation contours are from the E-OBS data. Contour spacing is 250 m.

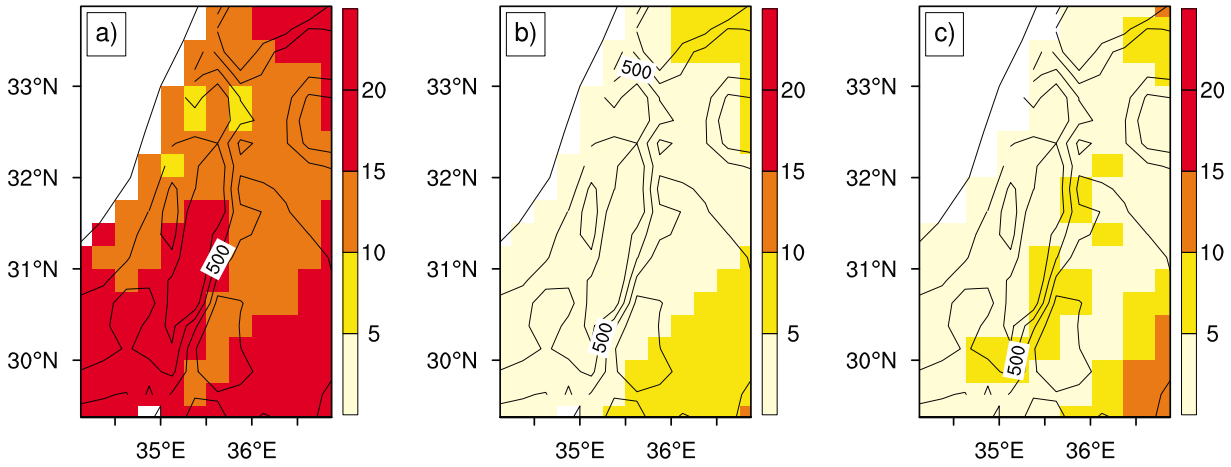

Figure 3. Trend (in days) in warm spell duration index for summer season (JJA) for 2021–2050 as compared with 1961–1990. (a) MM5/HadCM3, (b) MM5/ECHAM5(1), and (c) RegCM3/ECHAM5(3). Elevation contours are from the E-OBS data. Contour spacing is 250 m.

of between 1°C and 2°C, while the ECHAM5/RegCM model combination shows a middle range 1.5°C–2.5°C increase over the whole area. All of the simulations suggest a more intense warming inland as opposed to the coast, perhaps because of the modifying effects of sea breezes.

[15] Similar to Figure 2, Figure 3 shows the trend of the warm spell duration index for the summer months over the study region and for the different model simulation combinations. Here the Hadley driven model shows an intense increase of 12–20 events, while the two ECHAM5 driven models indicate a much more modest increase of up to 8 days. Part of difference in the results can be attributed to the difference in the driving GCM models, ECHAM5 and HadCM3. This can be attributed to the difference in the driving GCMs. The Hadley simulation has been shown to exhibit a steeper temperature increase in general until 2100 (3.5°C) *IPCC* [2007a]. *Trnka et al.* [2007] and in particular in the summer monthly temperature in central Europe as compared with the ECHAM5-MPI (3°C) [*Krichak et al.*, 2011, Table 2].

3.3. Absolute and Percentile-Based Precipitation Indices

[16] Figures 4 and 5 show the simulated changes in extreme precipitation amounts and events for the October–April wet season. While for the temperature indices the GCM model seemed to play a significant role in the intensity of the trends, for precipitation, the choice of RCM is important. In complex terrain RCM models still depict quite large biases in precipitation statistics [e.g., *Schmidli et al.*, 2007; *Smiatek et al.*, 2009]. In both MM5 simulations, the CDD in the north is extended by 3 days and more while the RegCM simulation shows a more moderate increase of 1–2 days. The models all agree with regard to the southern region of extended dry periods by 3 or more days. For the CWD, all models show little or no change in the duration in the south, but the RegCM simulations suggests shorter wet periods in the north of up to one day. Figures 6 and 7 show the pdfs of wet season percentile-based precipitation indices in the A and B regions. Both 75% (Figure 6) and 90% (Figure 7) values are shown. For both areas, the curve shifts

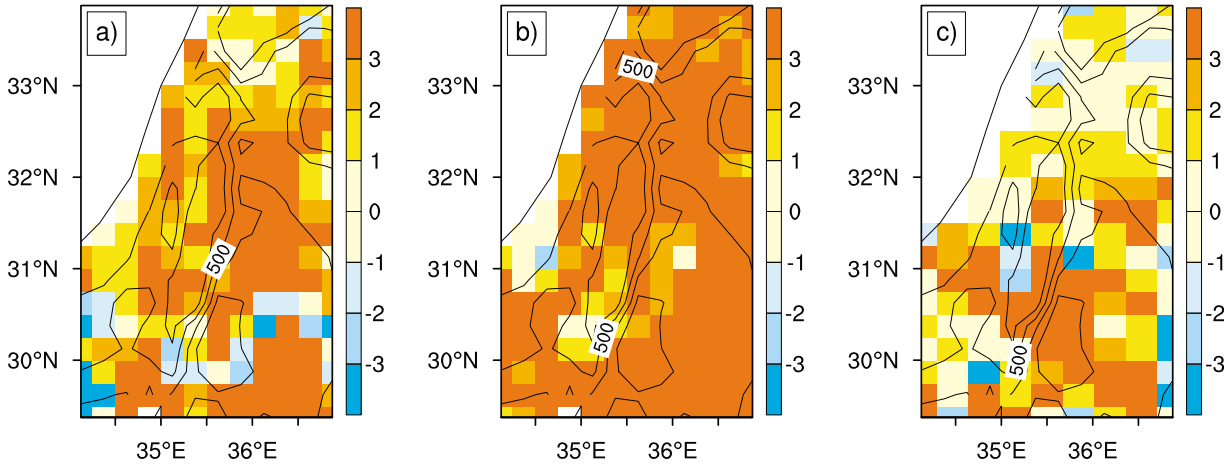

Figure 4. Simulated change in consecutive dry days for October–April 2021–2050 as compared with 1961–1990. (a) MM5/HadCM3, (b) MM5/ECHAM5(1), and (c) RegCM3/ECHAM5(3). Elevation contours are from the E-OBS data. Contour spacing is 250 m.

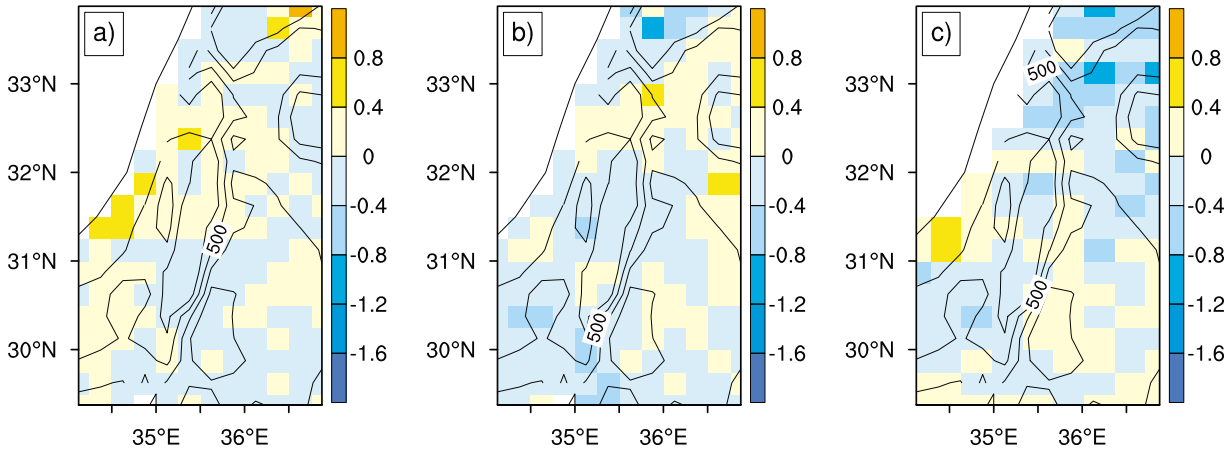

Figure 5. Simulated change in consecutive wet days for October–April 2021–2050 as compared with 1961–1990. (a) MM5/HadCM3, (b) MM5/ECHAM5(1), and (c) RegVM3/ECHAM5(3). Elevation contours are from the E-OBS data. Contour spacing is 250 m.

to the right for the amount of precipitation that falls on extremely rainy days, suggesting an increase in the amount of rain falling during the extreme events. Another indicator of changes in extreme rainfall can be seen in the number of days with more than 10 mm or 20 mm per day at a single location. We have not shown these results in the figures; however, it is interesting to note that the models show a larger spread, or interannual variability, in area A than the observed data. For both the A and B regions the curve for R10 shifts to the left in the future, indicating a marked decrease in the number of days with 10 mm or more rainfall. The same is true for the R20 indices for the A region, however for the B region, there is little change. This supports the changes indicated by the percentile changes in Figures 6 and 7.

3.4. Impacts of Expected Change

[17] In addition to the direct effects of rainfall changes on the number of consecutive wet days and consecutive dry days, these trends have important implications for agricultural decisions as well as understanding changes in expected soil moisture and evaporation. The decrease in average rainfall combined with an increase in heavy rain days or rainy periods suggests a shift in the patterns of rainfall distribution. Less light rainy days and more heavy rain days have implications for crop growing both in terms of the seasons available for planting and the types of crops that can be planted efficiently. Also in terms of water management, the rate of infiltration into the aquifers will change as soil moisture and conductivity is altered. Also, the chance of flooding increases with potentially more water lost to the sea. For the Sea of Galilee, the most important water resource in the region, the changes in temperature and wind which effect evaporation along with the changes in rainfall threaten to change the biological makeup of this natural reservoir [*Rimmer et al.*, 2011; *Hambright et al.*, 1994]. In addition, some natural plant communities may become vulnerable to invasive species because of reduced rainfall [*Har-Edom and Sternberg*, 2010].

[18] With regard to temperature increase, the biological diversity and distribution of mammals in some regions may be impacted as some species are not able to sustain the higher temperatures and extended hot, dry spells [*Steinitz et al.*, 2008]. The increased warm spells are also expected to have negative health impacts on the densely populated centers located in the center and south of the region, in area C (See Figure 1). Figure 8 shows how both summer and

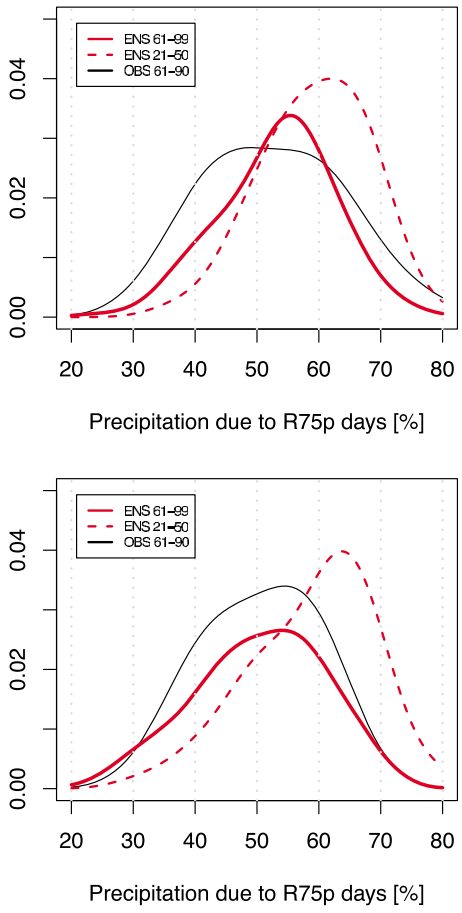

Figure 6. Probability distributions for R75pTOT in areas (top) A and (bottom) B.

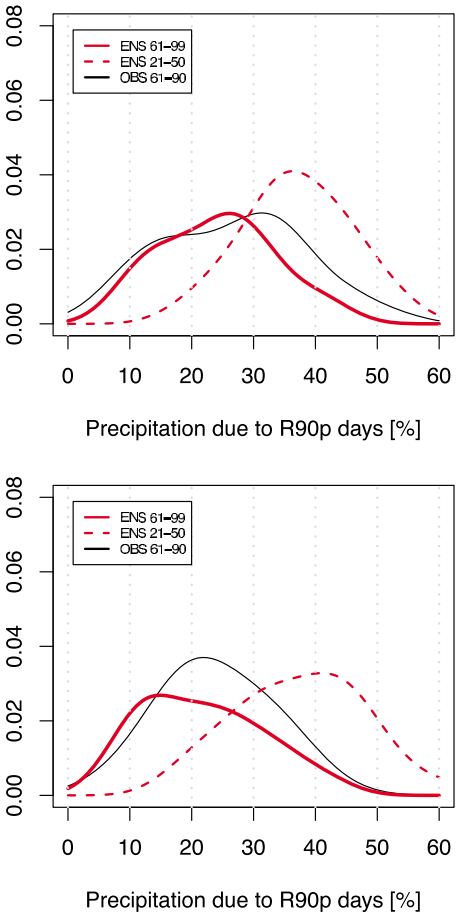

Figure 7. Probability distributions for R90pTOT in areas (top) A and (bottom) B.

winter maximum temperatures are projected to shift in that area, and Figure 9 shows how the minimum temperatures are projected to shift. Though the median summer maximum temperature seems to stay stable (the peak) the shift toward the right in the tails suggests that there will be more years with higher than median temperatures. For winter, the main change can be seen in the extension of the right tail, and decrease in median probabilities. This shift indicates

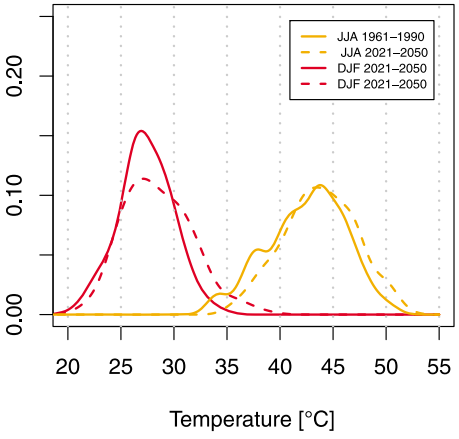

Figure 8. Probability distributions for TXx in area C winter and summer seasons.

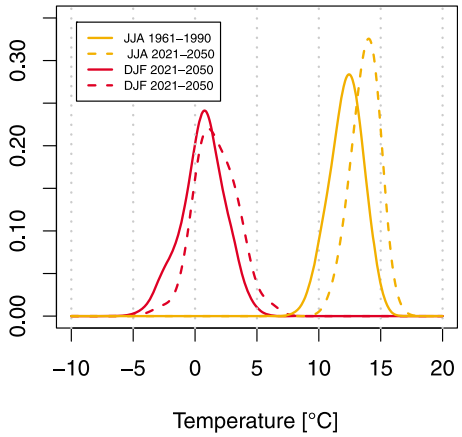

Figure 9. Probability distributions for TNx in area C winter and summer seasons.

that according to the model simulations the years with lower maximums will stay the same but the probability of a median year will decrease with an increase in years with warmer winters. This could have negative impacts on deciduous fruit trees and other crops which require a sufficient period of cold temperature to break winter dormancy [*Linvill*, 1990; *Saure*, 1985]. In their analysis of the 2006 heat wave over California with a similar Mediterranean-type climate, *Gershunov et al.* [2009] have shown that nighttime heat waves have intensified since the 1980s and they may have even higher impacts on human health. Compared to the maximum temperature, simulated changes in the daily minimum temperature (Figure 9) indicate a much higher increase of the daily minimum temperature in summer and the future period 2021–2050.

4. Conclusions

[19] We have presented results for expected changes in extreme rainfall and temperature parameters for a region in the Middle East. Previous analysis has shown consistent reductions in annual rainfall and increases in average temperature. Here we focus on changes in frequency of extreme events as they have vast implications across many sectors of society. Model specific results as well as ensemble averages are depicted in various formats so that the most appropriate representations can be chosen and understood by the impact community. In the presented model simulations it is interesting to note the agreement and differences between both the global driving models, the regional modeling schemes chosen as well as the different regions evaluated. For temperature data, it seems that the most important factor in trends and changes is the chosen Global Model, as discussed above. The Hadley GCM results are consistently warmer than the ECHAM5 results which is evident in the variability between model runs. All model results have a similar east–west gradient with more moderate increase occurring near the coastline, perhaps impacted by the sea breeze. For precipitation, the choice of the regional model plays an important role. This seems reasonable as much of the rainfall is orographic and highly dependent on local and regional processes which are not well defined in the global models. Both regional models used in this study agree about changes in

precipitation in the south (moderate change) but there is a difference in the north, the area critical to the water resources of the region. The trend determined according to the results of the experiment with the RegCM demonstrates little change in the CDD length and decrease in CWD length while the MM5 shows the opposite, little change in CWD length and an increase in CDD length. This difference in the relative importance of the global and regional model to the different parameters has important implication for future climate research and is being addressed in detail in a complementary research.

[20] **Acknowledgments.** We acknowledge the E-OBS data set from the EU-FP6 project ENSEMBLES (http://www.ensembles-eu.org) and the data providers in the ECA&D project (http://eca.knmi.nl). The authors thank the Leibniz-Rechenzentrum, Garching, for providing access to the HLRB II supercomputer. The study was partially funded by the German Federal Ministry of Science and Education (BMBF) within the GLOWA-JORDAN project.

References

Alexander, L. V., et al. (2006), Global observed changes in daily climate extremes of temperature and precipitation, *J. Geophys. Res.*, *111*, D05109, doi:10.1029/2005JD006290.

Alpert, P., et al. (2002), The paradoxical increase of Mediterranean extreme daily rainfall in spite of decrease in total values, *Geophys. Res. Lett.*, *29*(11), 1536, doi:10.1029/2001GL013554.

Alpert, P., S. Krichak, H. Shafir, D. Haim, and I. Osetinsky (2008), Climatic trends to extremes employing regional modeling and statistical interpretation over the E. Mediterranean, *Global Planet. Change*, *63*, 163–170, doi:0.1016/j.gloplacha.2008.03.003.

Chen, F., and J. Dudhia (2001), Coupling an advanced land surface hydrology model with the Penn State/NCAR MM5 modeling system. Part I: Model implementation and sensitivity, *Mon. Weather Rev.*, *129*, 569–585.

Collins, M. (2007), Ensembles and probabilities: A new era in the prediction of climate change, *Philos. Trans. R. Soc. A*, *365*, 1957–1970.

Díez, E., C. Primo, J. A. García-Moya, J. M. Gutierrez, and B. Orfila (2005), Statistical and dynamical downscaling of precipitation over Spain from DEMETER seasonal forecasts, *Tellus, Ser. A*, *57*, 409–423, doi:10.1111/j.1600-0870.2005.00130.x.

Gershunov, A., D. Cayan, and S. Iacobellis (2009), The great 2006 heat wave over California and Nevada: Signal of an increasing trend, *J. Clim.*, *22*, 6181–6203.

Giorgi, F., and P. Lionello (2008), Climate change projections for the Mediterranean region, *Global Planet. Change*, *63*, 90–104, doi:10.1016/j.gloplacha.2007.09.005.

Gordon, C., C. Cooper, C. A. Senior, H. Banks, J. M. Gregory, T. C. Johns, J. F. B. Mitchell, and R. A. Wood (2000), The simulation of SST, sea ice extents and ocean heat transports in a version of the Hadley Centre coupled model without flux adjustments, *Clim. Dyn.*, *16*, 147–168, doi:10.1007/s003820050010.

Gvirtsman, C. (2002), *Water Resources of Israel*, Yad Ben Tsvi, Jerusalem.

Hambright, K. D., M. Gophen, and S. Serruya (1994), Influence of long-term climatic changes on the stratification of a subtropical, warm monomictic lake, *Limnol. Oceanogr.*, *39*, 1233–1242.

Har-Edom, O.-L., and M. Sternberg (2010), Invasive species and climate change: *Conyza canadensis* (l.) Cronquist as a tool for assessing the invasibility of natural plant communities along an aridity gradient, *Biol. Invasions*, *12*, 1953–1960, doi:10.1007/s10530-009-9640-z.

Haylock, M., N. Hofstra, A. K. Tank, E. Klok, P. Jones, and M. New (2008), A European daily high-resolution gridded data set of surface temperature and precipitation for 1950–2006, *J. Geophys. Res.*, *113*, D20119, doi:10.1029/2008JD010201.

Hertig, E., and J. Jacobeit (2008), Downscaling future climate change: Temperature scenarios for the Mediterranean area, *Global Planet. Change*, *63*, 127–131.

Intergovernmental Panel on Climate Change (IPCC) (2007a), *Climate Change 2007: The Physical Science Basis. Summary for Policymakers*, edited by S. Solomon et al., Cambridge Univ. Press, Cambridge, U. K.

Intergovernmental Panel on Climate Change (IPCC) (2007b), *Climate Change 2007: Impacts, Adaptation, and Vulnerability. Contribution of Working Group II to the Fourth Assessment Report of the Intergovernmental Panel on Climate Change*, edited by M. L. Parry et al., Cambridge Univ. Press, Cambridge, U. K.

Karl, T., N. Nicholls, and A. Ghazi (1999), CLIVAR/GCOS/WMO workshop on indices and indicators for climate extremes: Workshop summary, *Clim. Change*, *42*, 3–7.

Krichak, S., P. Alpert, and P. Kunin (2010), Numerical simulation of seasonal distribution of precipitation over the eastern Mediterranean with a RCM, *Clim. Dyn.*, *34*, 47–59.

Krichak, S., J. Breitgand, R. Samuels, and P. Alpert (2011), A double-resolution transient RCM climate change simulation experiment for near-coastal eastern zone of the eastern Mediterranean region, *Theor. Appl. Climatol.*, *103*(1–2), 167–195.

Kunstmann, H., P. Suppan, A. Heckl, and A. Rimmer (2007), Regional climate change in the Middle East and impact on hydrology in the Upper Jordan catchment, in *Quantification and Reduction of Predictive Uncertainty for Sustainable Water Resources Management: Proceedings of Symposium HS2004 at IUGG2007, Perugia, July 2007*, *IAHS Publ.*, *313*, 141–149.

Linvill, D. (1990), Calculating chilling hours and chill units from daily maximum and minimum temperature observations, *HortScience*, *25*(1), 14–16.

Lopez, A., F. Fung, M. New, G. Watts, A. Weston, and R. L. Wilby (2009), From climate model ensembles to climate change impacts and adaptation: A case study of water resource management in the southwest of England, *Water Resour. Res.*, *45*, W08419, doi:10.1029/2008WR007499.

Mariotti, A., N. Zeng, J. Yoon, V. Artale, A. Navarra, P. Alpert, and L. Li (2008), Mediterranean water cycle changes: Transition to drier 21st century conditions in observations and CMIP3 simulation, *Environ. Res. Lett.*, *3*, 1–8, doi:10.1088/1748-9326/3/4/044001.

Menzel, L., J. Koch, J. Onigkeit, and R. Schaldach (2009), Modelling the effects of land-use and land-cover change on water availability in the Jordan River region, *Adv. Geosci.*, *21*, 73–80, doi:10.5194/adgeo-21-73-2009.

Mitchell, T. D., and P. D. Jones (2005), An improved method of constructing a database of monthly climate observations and associated high-resolution grids, *Int. J. Climatol.*, *26*, 693–712, doi:10.1002/joc.1181.

Mitchell, T. D., T. R. Carter, P. D. Jones, M. Hulme, and M. New (2004), A comprehensive set of high-resolution grids of monthly climate for Europe and the globe: The observed record (1901–2000) and 16 scenarios (2001–2100), *Tyndall Cent. Work. Pap. 55*, Tyndall Cent., Norwich, U. K.

Pal, J., et al. (2007), Regional climate modeling for the developing world: The ICTP RegCM3 and RegCNET, *Bull. Am. Meteorol. Soc.*, *88*, 1395–1409.

Peterson, T., et al. (2001), Report on the activities of the working group on climate change detection and related rapporteurs 1998–2001, *Rep. WMO-TD 1071*, 143 pp., World Meteorol. Organ., Geneva, Switzerland.

Rimmer, A., G. Gal, T. Opher, Y. Lechinshy, and Z. Yacobi (2011), Mechanisms of long-term variations of the thermal structure in a warm lake, *Limnol. Oceanogr.*, *56*(3), 974–988, doi:10.4319/lo.2011.56.3.0974.

Robertson, A. W., A. V. M. Ines, and J. W. Hansen (2007), Downscaling of seasonal precipitation for crop simulation, *J. Appl. Meteorol. Climatol.*, *46*, 677–693.

Roeckner, E., R. Brokopf, M. Esch, M. Giorgetta, S. Hagemann, L. Kornblueh, E. Manzini, U. Schlese, and U. Schulzweida (2006), Sensitivity of simulated climate to horizontal and vertical resolution in the ECHAM5 atmosphere model, *J. Clim.*, *19*, 3771–3791, doi:10.1175/JCLI3824.1.

Saaroni, H., B. Ziv, and P. Alpert (2003), Long-term variations in summer temperatures over the eastern Mediterranean, *Geophys. Res. Lett.*, *30*(18), 1946, doi:10.1029/2003GL017742.

Samuels, R., A. Rimmer, A. Hartman, S. Krichak, and P. Alpert (2010), Climate change impacts on Jordan River flow: Downscaling application from a regional climate model, *J. Hydrometeorol.*, *11*(4), 860–879.

Saure, M. (1985), Dormancy release in deciduous fruit trees, *Hortic. Rev.*, *7*, 239–300.

Schmidli, J., C. M. Goodess, C. Frei, M. R. Haylock, Y. Hundecha, J. Ribalaygua, and T. Schmith (2007), Statistical and dynamical downscaling of precipitation: An evaluation and comparison of scenarios for the European Alps, *J. Geophys. Res.*, *112*, D04105, doi:10.1029/2005JD007026.

Smiatek, G., H. Kunstmann, R. Knoche, and A. Marx (2009), Precipitation and temperature statistics in high-resolution regional climate models: Evaluation for the European Alps, *J. Geophys. Res.*, *114*, D19107, doi:10.1029/2008JD011353.

Smiatek, G., H. Kunstmann, and A. Heckl (2011), High resolution climate change simulations for the Jordan River area, *J. Geophys. Res.*, *116*, D16111, doi:10.1029/2010JD015313.

Steinitz, H., T. Dayan, and Y. Yom-Tov (2008), Projected shifts in the distribution of Israeli mammals in different climate change scenarios, paper presented at 45th Meeting, Isr. Zool. Soc., Michmoret, Israel.

Stott, P. A., and C. E. Forest (2007), Ensemble climate predictions using climate models and observational constraints, *Philos. Trans. R. Soc. A*, *365*, 2029–2052, doi:10.1098/rsta.2007.2075.

Tal, A. (2006), Seeking sustainability: Israel's evolving water management strategy, *Science*, *313*, 1081–1084.

Trnka, M., et al. (2007), Expected changes in agroclimatic conditions in central Europe, *Clim. Change*, *108*, 261–289, doi:10.1007/s10584-011-0025-9 .

van den Besselaar, E., M. Haylock, G. van der Schrier, and A. M. G. Klein Tank (2011), A European daily high-resolution observational gridded data set of sea level pressure, *J. Geophys. Res.*, *116*, D11110, doi:10.1029/2010JD015468.

World Climate Research Programme (2009), Evaluating and Improving Regional Climate Projections, Toulouse, France, 11–13 February 2009, *WCRP Informal Rep. 5/2009*, Geneva, Switzerland.

World Meteorological Organization (2009), Guidelines on analysis of extremes in a changing climate in support of informed decisions for adaptation, *Tech. Rep. 72*, Geneva, Switzerland.

Zhang, X., et al. (2005), Trends in Middle East climate extreme indices from 1950 to 2003, *J. Geophys. Res.*, *110*, D22104, doi:10.1029/2005JD006181.

P. Alpert, S. Krichak, and R. Samuels, Department of Geophysics and Planetary Sciences, Tel Aviv University, PO Box 34090, Tel Aviv 69978, Israel.

H. Kunstmann and G. Smiatek, Institute for Meteorology and Climate Research, Karlsruhe Institute of Technology, Kreuzeckbahnstr. 19, D-82467 Garmisch-Partenkirchen, Germany. (gerhard.smiatek@kit.edu)